



Endoscopic Fluorescence-Guided Surgery for Sinonasal Cancer Using an Antibody-Dye Conjugate

Zachary P. Hart*; Naoki Nishio, MD, PhD* ; Giri Krishnan, MD; Guolan Lu, PhD; Quan Zhou, PhD; Shayan Fakurnejad, BS; Peter John Wormald, MD; Nynke S. van den Berg, PhD; Eben L. Rosenthal, MD ; Fred M. Baik, MD

Objective: Endoscopic resection of sinonasal squamous cell carcinoma has become the standard of care, but challenges remain in obtaining clear resection margins. The current study evaluated the feasibility of endoscopic fluorescence-guided surgery (FGS) to improve surgical resection in a human sinus surgical model.

Methods: A fluorescence endoscope optimized for near-infrared (NIR) fluorescence detection was evaluated in a phantom study. Various endoscope diameters (4 and 10 mm) and viewing angles (0, 30, and 45 degrees) were evaluated to determine the sensitivity of the system for IRDye800CW detection at various working distances (1–5 cm). Endoscopic FGS was then validated in a three-dimensional human sinus surgical model to which squamous cell tumors derived from mice were inserted. Mice had received intravenous panitumumab-IRDye800CW and upon fluorescence-guided tumor resection, mean fluorescence intensity (MFI) and tumor-to-background ratio (TBR) were calculated in situ and ex vivo settings.

Results: A significantly higher fluorescence intensity was found when using the 10-mm diameter endoscope compared to the 4mm diameter endoscope ($P < .001$). No significant difference in MFI was found among the viewing angles of the 4-mm diameter endoscope. Using the human sinus model, the highest MFI and TBR were obtained at a 1-cm working distance compared to longer working distances.

Conclusion: We demonstrate that clinically acceptable TBRs were obtained with several working distances to discriminate tumor tissue from adjacent normal tissue in a human sinus model, and that endoscopic FGS may have great potential in identifying residual tumor tissue regions during surgery.

Key Words: Fluorescence-guided surgery, endoscope, near-infrared, sinonasal cancer, squamous cell carcinoma.

Laryngoscope, 130:2811–2817, 2020

This is an open access article under the terms of the Creative Commons Attribution-NonCommercial License, which permits use, distribution and reproduction in any medium, provided the original work is properly cited and is not used for commercial purposes.

From the Department of Otolaryngology (Z.P.H., N.N., G.K., G.L., Q.Z., S.F., N.S.V., E.L.R., F.M.B.), Stanford University School of Medicine, Stanford, California, U.S.A.; the Department of Otorhinolaryngology (N.N.), Nagoya University Graduate School of Medicine, Nagoya, Aichi, Japan; and the Department of Surgery–Otorhinolaryngology, Head and Neck Surgery (G.K., P.J.W.), University of Adelaide, Adelaide, Australia.

Additional supporting information may be found in the online version of this article.

Editor's Note: This Manuscript was accepted for publication on December 08, 2019.

*These contributed equally to this work and therefore share first authorship.

This work was supported in part by the Stanford Comprehensive Cancer Center, the Stanford University School of Medicine Medical Scholars Program, the Netherlands Organization for Scientific Research (Rubicon; 019.171LW.022), the National Institutes of Health and the National Cancer Institute (R01CA190306), the Stanford Molecular Imaging Scholars (SMIS) program (T32 CA118681), the Garnett Passe and Rodney Williams Memorial Foundation, and the Fulbright Commission, and institutional equipment loans from KARL STORZ SE & Co KG and LI-COR Biosciences Inc.

Eben L. Rosenthal acts as consultant for LI-COR Biosciences Inc. and has equipment loans from this company. All other authors declare no conflict of interest.

Send correspondence to Fred M. Baik, MD, Department of Otolaryngology–Head and Neck Surgery, 900 Blake Wilbur Drive, Palo Alto, CA 94304. Email: fbaik@stanford.edu

DOI: 10.1002/lary.28483

INTRODUCTION

Sinonasal squamous cell carcinoma (SNSCC) is the most common histology in malignant sinonasal tumors.^{1,2} Surgical resection is considered the standard of care treatment for SNSCC, and complete resection with tumor-free margins provides optimal survival.³ Recent studies have demonstrated the usefulness and feasibility of an endoscopic approach for malignant sinonasal tumors with acceptable survival outcomes and low rate of surgical complications.^{4–6} However, while endoscopy allows for minimally invasive surgery and direct visualization of the surgical field, clear resection margins can be difficult to ascertain due to a narrow field of view and the inability to palpate tumor edges. Consequently, rates of positive margins for endoscopic surgery for SNSCC are high (22–30%), which can result in increased local recurrence and decreased survival.^{7,8}

Fluorescence-guided surgery (FGS) is increasingly being studied as a guide to differentiate tumor tissue from normal tissue in an intraoperative setting.⁹ Although several agents are under active clinical study,^{10–13} we investigated the anti-epidermal growth factor receptor (EGFR) antibody-dye conjugate panitumumab-IRDye800CW, which has demonstrated a high sensitivity and specificity of squamous cell carcinoma (SCC) detection in patients with head and neck cancer.^{14–18} We hypothesize that translating this

technique to endoscopic surgery may improve discrimination of tumor tissue from adjacent normal tissue. This would ultimately allow for more precise visualization of the tumor margins and reduce incomplete tumor resection. Thus, the objective of this study was to evaluate the potential clinical utility of the endoscopic sinonasal FGS technique in a novel human sinus surgical model and to determine the optimal surgical conditions for fluorescence detection.

MATERIALS AND METHODS

Endoscopic Fluorescence Imaging System

The endoscopic near-infrared (NIR) fluorescence imaging system included a D-Light P Xenon light source with ICG filters and an Image1S H3-Z FI camera. Other components on the device were the Image1 S connect platform, the Image1 S H3-link, a Storz Aida HD Connect, and a fiber optic light cable connecting the light source and rigid Hopkins telescopes (KARL STORZ SE & Co KG, Tuttlingen, Germany). Using a foot-switch, the system allows a switchover between fluorescence and standard white light mode.

Shown in Figure 1 are the endoscopes that were evaluated. Three 4-mm diameter, 18-cm long endoscopes (0, 30, and 45 degrees) and two 10-mm diameter, 31-cm long, endoscopes (0 and 30 degrees) were evaluated. All of the endoscopes had built-in filters for NIR light detection, with the detected fluorescence signal being displayed on-screen as a blue signal overlaid onto a bright field image. Images taken with the endoscopic imaging device were compared with a closed-field fluorescence imaging device (Pearl Trilogy Imaging System; LI-COR Biosciences Inc., Lincoln, NE, USA). The closed-field device shields

itself from ambient light, allowing for consistent fluorescence imaging and served as a “gold-standard” fluorescence imaging device in this study, in a manner similar to as previously reported.¹⁸

Sensitivity to IRDye800CW

To determine the sensitivity of the device to NIR fluorescence detection of panitumumab-IRDye800CW, a 20-step 1:2 dilution range, ranging 4.58 mM to 3.94 pM, was generated of IRDye800CW carboxylate (LI-COR Biosciences Inc.) in water. For reference, the dilution range was first measured in the closed-field imaging device. Subsequently, the three rigid 4mm diameter endoscopes (0, 30, and 45 degrees; Fig. 1) and two 10-mm diameter endoscopes (0 and 30 degrees) were used to measure fluorescence signals for all concentrations of dye to determine, quantitatively and qualitatively, the sensitivity of the device, in a manner similar to as previously reported.¹⁹ To determine the optimal working distance of the endoscope (ie, the working distance at which the highest sensitivity was reached) the experiment was performed at working distances ranging 1–5 cm.

Endoscopic Sinus Surgery Model

Nude (nu/nu) female mice, aged 6–8 weeks (Charles River Laboratories, Wilmington, MA, USA), were obtained and housed in accordance with our Institutional Animal Care and Use Committee (IACUC) guidelines. All experiments were conducted after review and approval of the institution’s IACUC guidelines. To generate the orthotopic head and neck squamous cell carcinoma (HNSCC) model, mice (n = 4) were injected with SCC-1 cells (0.5×10^6 ; in 25 μ L PBS; ATCC, Manassas, VA) in the floor-of-

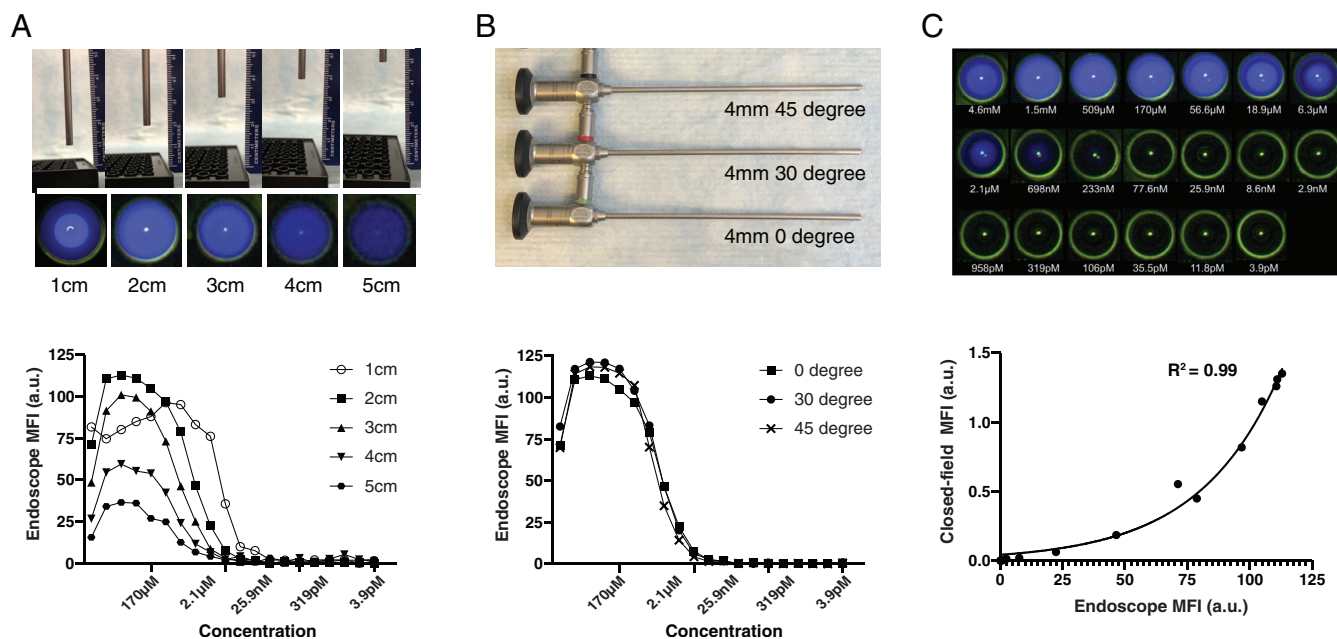


Fig. 1. IRDye800CW sensitivity testing of an endoscopic fluorescence imaging system. A) top: Phantom setup; bottom: Fluorescence signal intensities as detected with the 4-mm diameter endoscope (0 degree) at various working distances (1–5 cm). B) top: Tested 4-mm diameter, 18-cm long, endoscopes with 0, 30, and 45 degrees; bottom: 4-mm diameter endoscopes (0, 30, 45 degrees) were evaluated at 2 cm working distance for their sensitivity in detecting IRDye800CW. C) top: Visual impression of the fluorescence signal detected with 0 degree, 4-mm diameter endoscope; bottom: Fluorescence signals (MFI) detected with 4-mm diameter endoscope (0 degree) was plotted against the MFIs measured with the closed-field imaging device. [Color figure can be viewed in the online issue, which is available at www.laryngoscope.com.]

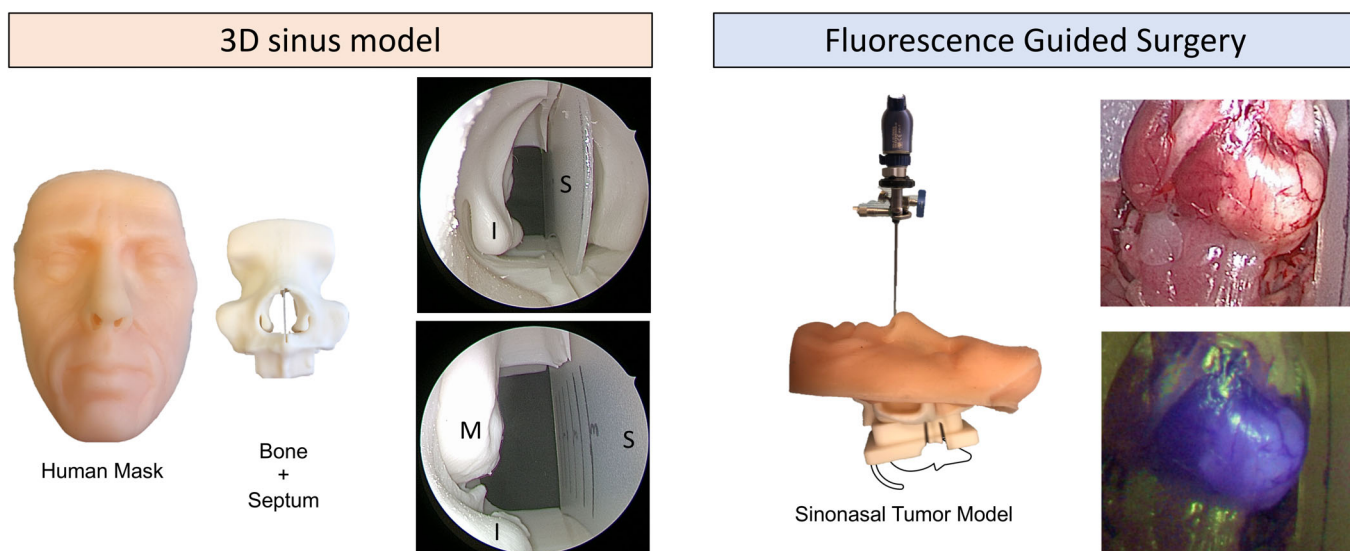


Fig. 2. Clinically relevant surgical sinus model. Left: Three-dimensional sinus model—components of the sinus model with two endoscopic images. S = septum; I = inferior turbinate; M = middle turbinate. Right: Fluorescence-guided surgery—representative images acquired with the 4-mm diameter endoscope (0 degree). Bright field (top) and fluorescence images (bottom) are collected with the endoscope. [Color figure can be viewed in the online issue, which is available at www.laryngoscope.com.]

mouth using a 30-G insulin syringe. Tumor growth was followed for 2–3 weeks by direct visual inspection and palpation, after which the mice were systemically injected with 100 μ g of GMP-produced panitumumab-IRDye800CW.¹⁴ Mice were sacrificed 48 hours post-injection after which the skin overlying the floor of the mouth was removed and imaging in the closed-field device was performed to verify presence of panitumumab-IRDye800CW.

In order to simulate the anatomic and light conditions of SNSCC resection, sacrificed mice were placed in an anatomically accurate three-dimensional sinus model (sinus model otorhino neuro trainer; Pro Delphus, Pernambuco, Brazil).²⁰ An overview of the experimental setup is given in Figure 2. Tumors were then resected under guidance of the endoscopic imaging using the 0 degree, 4-mm diameter, endoscope whereby various working distances (1, 2, and 3 cm) were assessed. Upon completion of resection, a second closed-field fluorescence image was acquired to verify the complete removal of the tumor tissue.

To determine the smallest detectable size of tumor tissue, excised tumor tissue and normal muscle were divided into parts, varying in weight from 0.2 to 20 mg (Fig. 5). Each piece was imaged using the fluorescence endoscopic imaging device, and for verification, each piece was also imaged in the closed-field device.

Histopathology

During resection of the tumor tissue from the mice, representative primary tumor tissue, tumor-to-normal margin tissue and wound-bed tissue was collected, formalin-fixed and paraffin embedded, after which blank slides (4- μ m thickness) were obtained for a hematoxylin and eosin (H&E) stain. Subsequent immunohistochemistry was also conducted to assess for epidermal growth factor (EGFR) expression using an anti-EGFR antibody (clone EP38Y, Thermo Fisher Scientific, Waltham, MA, USA).¹⁴

Fluorescence Microscopy

For fluorescence microscopy, selected tissue slides were deparaffinized, and the nuclei were counterstained with

4',6-diamidino-2-phenylindole (DAPI, Prolong Diamond, Thermo Fisher Scientific). Stained slides were dried overnight, in the dark, and imaged using a custom setup inverted digital fluorescence microscope (DM6B, Leica Biosystems, Wetzlar, Germany) equipped with a highly sensitive Leica DFC9000GT camera (4.2-M pixel sCMOS camera), a metal halide LED light source (X-Cite 200DC, Excelitas Technologies, Waltham, MA, USA) for DAPI imaging, and a xenon arc lamp LB-LS/30 (Sutter Instrument, Novato, CA, USA) for NIR imaging of IRDye800CW. Image acquisition and processing was done using LAS X software (Leica Biosystems).

Image Quantification and Data Analysis

Endoscopic images that were acquired before, during, and after tumor resection were loaded into ImageJ (National Institutes of Health, Bethesda, MD, USA) to quantitatively assess the fluorescence signal in situ and ex vivo. Because the endoscopic imaging system presents the fluorescence signal as an overlay image whereby the fluorescence signal (in blue) is overlaid on the bright field image, acquired images were split into RGB color channels in ImageJ. Subsequently, the blue channel of each image was analyzed in ImageJ as being the “raw” fluorescence signal. Reference (“gold standard”) images acquired with the closed-field fluorescence-imaging device were analyzed using Image Studios software (LI-COR Biosciences Inc.).

For fluorescence signal quantification in both ImageJ and Image Studio, regions of interest (ROIs) were drawn around the area of interest and mean fluorescence intensities (MFIs, a.u.) were calculated. Tumor-to-background ratios (TBRs) were calculated by dividing tumor MFI by the normal tissue MFI.

Statistical Analysis

Descriptive statistics was performed using GraphPad Prism software (Version 6.0c; GraphPad Software, La Jolla, CA, USA). Data is presented as means with standard deviations for continuous variables. To compare the endoscope variants (diameter and

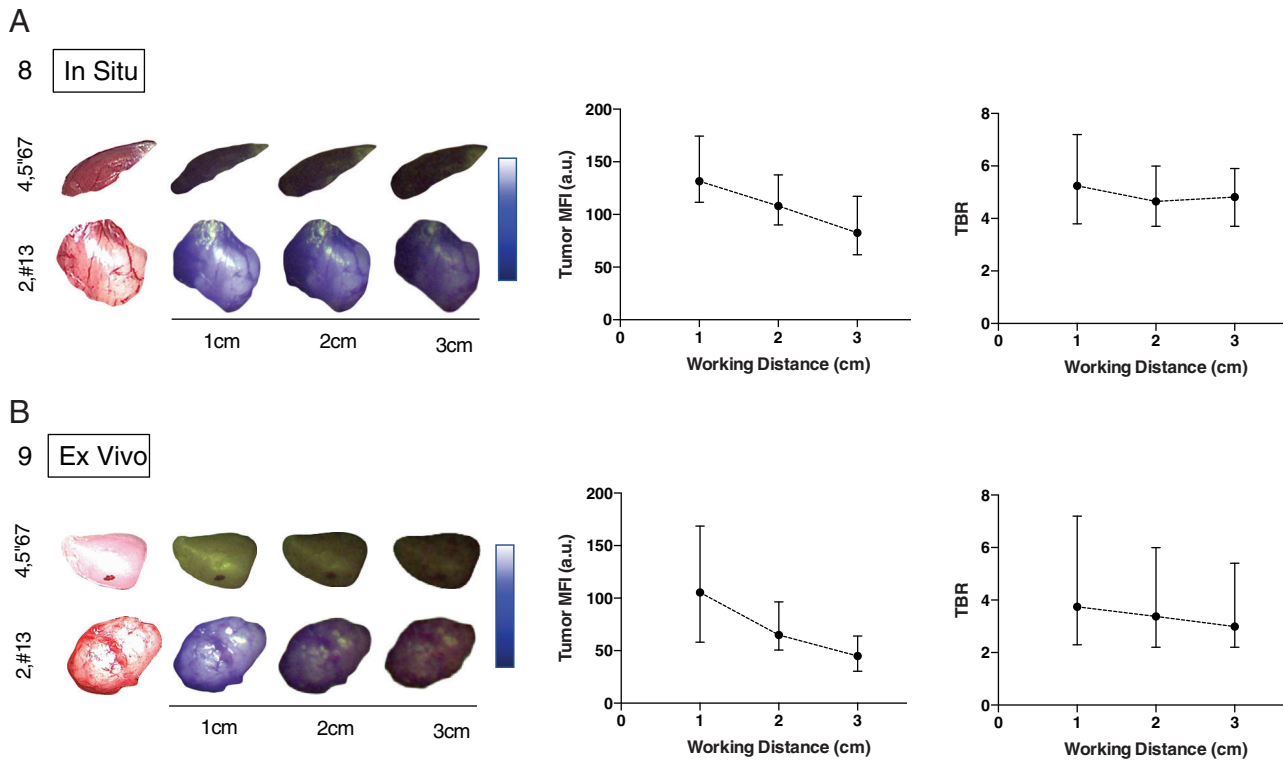


Fig. 3. Fluorescence signals and tumor-to-background ratio in situ and ex vivo setting measured at three working distances (1–3 cm). Images taken by the endoscopic fluorescence imaging system of in situ (A) and ex vivo (B) normal muscle and tumor tissue at three working distances (1–3 cm). [Color figure can be viewed in the online issue, which is available at www.laryngoscope.com.]

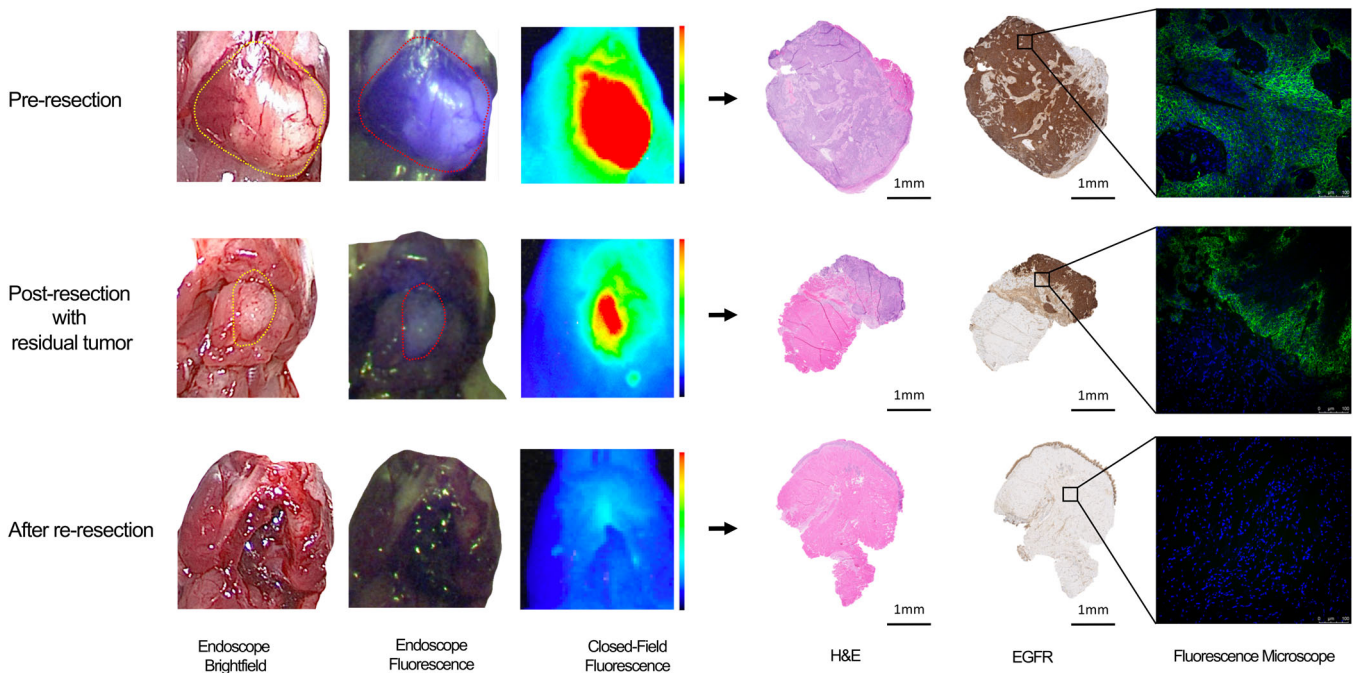


Fig. 4. Fluorescence-guided resection of tumor. Using the 4mm diameter endoscope (0 degrees), fluorescence and bright field images were acquired prior to resection, after initial resection, and after re-resection of residual tumor. Histopathology confirmed presence of EGFR in the excised tumor tissue, but not in the normal tissue. Via fluorescence microscopy presence of panitumumab-IRDye800CW was confirmed in the tumor tissue. [Color figure can be viewed in the online issue, which is available at www.laryngoscope.com.]

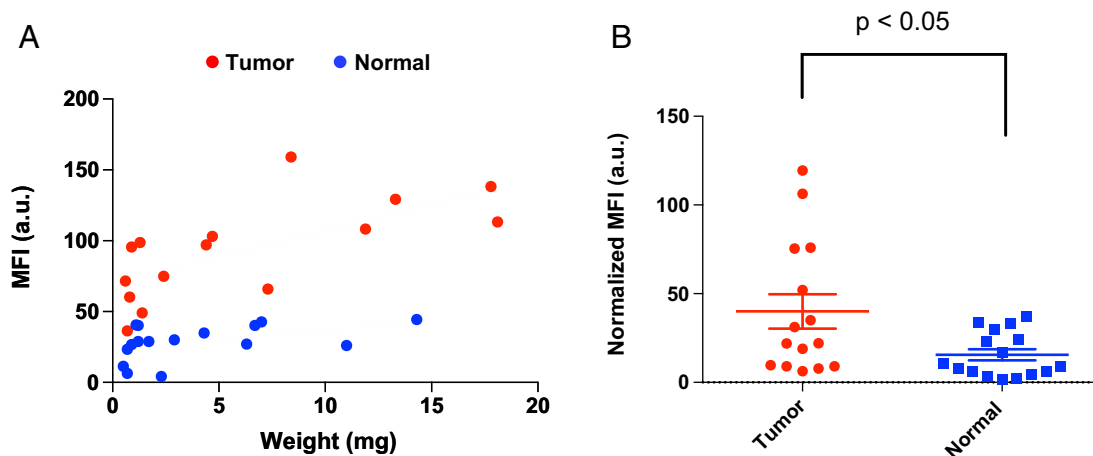


Fig. 5. Panitumumab-IRDye800CW uptake in tumor and normal tissue. A) Tumor and normal muscle were serially bisected into pieces, with the smallest piece being 0.6 mg, and the fluorescence signal was imaged using the 4-mm diameter endoscope (0 degrees). The mean fluorescence signal (MFI) was plotted as a function of weight (mg) of both tumor (red) and normal (muscle; blue) tissue samples. B) Upon normalization of the fluorescence signal, by dividing the measured MFI by the tissue weight, panitumumab-IRDye800CW distribution in tumor tissue was found to be significantly higher in tumor tissue compared to normal (muscle) tissue. [Color figure can be viewed in the online issue, which is available at www.laryngoscope.com.]

degree) in the phantom study, Wilcoxon matched-pairs signed rank test or Friedman test were used. Mann-Whitney U test was used for comparison of the tumor MFIs and normal tissue MFIs. Exponential regression analysis was performed on data comparing the two imaging systems. A *P*-value of .05 or less was considered statistically significant.

RESULTS

Ex-vivo Fluorescence Endoscopy Validation

Three 4-mm diameter endoscopes of varying angles of view (0, 30, and 45 degrees) were used to image the dilution range of 20 concentrations of IRDye800CW at five working distances ranging 1–5 cm to evaluate the sensitivity of the endoscopes. For the 4-mm diameter endoscope (0 degree), the highest and most reliable fluorescence signals were obtained at the 2-cm working distance (Fig. 1A); therefore, we determined 2 cm as the optimal working distance for our phantom study. In terms of the degree of 4mm diameter endoscopes, no differences were found in MFI when changing the angle of the endoscope (0, 30, and 45 degree; *P* = .17, Fig. 1B). Visually, at a working distance of 2 cm, the lowest concentration of dye that produced a visible fluorescence signal in the raw images was 698 nM (Fig. 1C). Fluorescence imaging data obtained with the endoscopic device strongly correlated to that of the closed-field imaging device ($R^2 = 0.99$, Fig. 1C), which indicated the robustness of the endoscopic fluorescence imaging system. When comparing between 4-mm and 10-mm diameter endoscopes, a significantly higher MFI was found when using the 10-mm diameter endoscope (*P* < .001, Supplementary Fig. 1).

Fluorescence Endoscopy Discriminates Tumor Tissue from Adjacent Surrounding Normal Tissue

To recreate the clinical environment, an in situ sinus model was employed and using the 0 degree, 4-mm diameter

endoscope we studied tumor visibility at various working distances (1–3 cm) and analyzed the tumor MFI and TBR in situ and ex vivo. In situ, a higher tumor MFI was found at the 1-cm working distance compared to the 2- or 3-cm working distances (mean MFI 131.6 a.u. vs. 108.0 a.u. and 82.6 a.u.), but similar TBRs were obtained for the three working distances (mean 5.2, 4.6, and 4.8, respectively) (Fig. 3A). Similar results were found, ex vivo, where tumors were imaged outside of the sinus model. Ex vivo, the MFI was also found to be highest at a working distance of 1 cm compared to the 2- or 3-cm working distances (mean; 110.5 a.u. vs. 75.4 a.u. and 51.6 a.u.) with TBR decreasing with increasing working distance (mean 3.7, 3.4, and 3.0, respectively) (Fig. 3B).

Fluorescence Endoscopy Identifies Residual Tumor Deposits

Using the human sinus model, the potential value of endoscopic FGS for tumor visualization and margin assessment for sinonasal surgery was assessed. Following tumor visualization (Fig. 4), an incomplete tumor resection was performed to evaluate whether or not the imaging device was sensitive enough to pick up residual tumor. As can be seen in Figure 4, residual tumor deposits could be clearly visualized and subsequently removed. In further assessment of excised tumor tissue pieces, the smallest piece of tumor tissue (0.6 mg) had a visible fluorescence signal and could be discriminated from normal tissue (Fig. 5A). A significantly higher MFI was found for tumor tissue when compared to normal tissue (mean: 40.0 vs. 15.6 a.u., *P* < .05, Fig. 5b), demonstrating this technique could clearly discriminate the tumor tissue from normal tissue even though the tumor deposits were very small. Imaging results with the endoscopic device were corroborated by the closed-field imaging device. Histology, including immunohistochemistry of EGFR, confirmed the presence of tumor at areas that were positive for fluorescence (Fig. 4).

DISCUSSION

For sinonasal cancers, complete resection with clear margins significantly impacts oncologic outcomes in patients treated with minimally invasive endoscopic resection.^{8,21} Despite the fact that intraoperative frozen margins are reliably interpreted for sinonasal tumors,²² a clear demarcation of tumor from normal tissue or inflamed polypoid tissues is difficult within the sinonasal cavity. In the current study we demonstrate that endoscopic fluorescence imaging can be sensitive and specific to detect the tumor after systemic administration of a NIR tumor-targeting agent. Moreover, clinically relevant TBRs were obtained with several working distances to discriminate the tumor from adjacent normal tissue in a human sinus model, highlighting the potential of this technique to identify residual tumor regions during surgery. Results of the current study are in line with previous studies in open-field FGS approaches for identification of tumor in an in vivo and an ex vivo setting.^{15,17}

The current study demonstrates that endoscopic imaging systems with NIR fluorescence-detection designed for ICG can be repurposed for use with IRDye800CW. Despite the consistency of the TBR at greater working distances in our model, the fluorescent signal (measured in MFI) was negatively correlated with working distance. The optimal working distance is thought to lie within 1–3 cm in a clinical setting; fluorescence imaging becomes brighter as the working distance is reduced and vice versa. However, there is an increase in light reflection off of tissue at shorter working distances, which may ultimately obscure tumor visualization in a surgical setting.

Endoscopes used for sinus surgery or endonasal skull base surgery generally have an outer diameter of 4 mm, whereas endoscopes with 10-mm diameter are common in the laparoscopic surgeries. Our results demonstrate the applicability of the FGS technique beyond open-field and laparoscopic applications (eg, in the abdominal cavity). Although the fluorescence signal obtained from 4-mm diameter endoscopes was less than the signal from 10-mm diameter endoscopes in our phantom experiments, a strong fluorescence signal with acceptable TBRs was achieved in the sinus surgery model using the 4-mm diameter endoscope. Interestingly, the fluorescence intensity was consistent with 0, 30, and 45 degrees of view angle in the phantom study, demonstrating the wide applicability of this technique, particularly for bulky and odd-shaped tumors.

Clinically, endoscopic FGS has emerged as a promising technique to improve surgical precision during tumor resection. Utilizing NIR fluorescence imaging using ICG with laparoscopic and robot-assisted surgery have improved oncologic outcomes reported in procedures such as hepatectomy,²³ nephrectomy,²⁴ hysterectomy,²⁵ and gastrectomy.²⁶ We and others have reported the feasibility and potential clinical benefits of FGS using antibody dye-based imaging for patients with solid tumors.^{10,11,13–18,27–31} Combining FGS with the advantages of a minimally invasive, endoscopic approach may hold the potential to reduce morbidity while ensuring adequate oncologic outcomes. However, this has yet to be further investigated and validated in large prospective trials.

CONCLUSION

We demonstrate that endoscopic imaging of a tumor-specific NIR imaging agent can discern tumor tissue from normal tissue in a preclinical model under a range of conditions with a clinically relevant TBR at working distances from 1–3 cm.

BIBLIOGRAPHY

1. Turner JH, Reh DD. Incidence and survival in patients with sinonasal cancer: a historical analysis of population-based data. *Head Neck* 2012;34:877–885.
2. Bhattacharyya N. Factors affecting survival in maxillary sinus cancer. *J Oral Maxillofac Surg* 2003;61:1016–1021.
3. Nishio N, Fujimoto Y, Fujii M, et al. Craniofacial resection for T4 maxillary sinus carcinoma: managing cases with involvement of the skull base. *Otolaryngol Head Neck Surg* 2015;153:231–238.
4. Kılıç S, Kılıç SS, Baredes S, et al. Comparison of endoscopic and open resection of sinonasal squamous cell carcinoma: a propensity score-matched analysis of 652 patients. *Int Forum Allergy Rhinol* 2018;8:421–434.
5. Rawal RB, Farzal Z, Federspiel JJ, Sreenath SB, Thorp BD, Zanation AM. Endoscopic resection of sinonasal malignancy: a systematic review and meta-analysis. *Otolaryngol Head Neck Surg* 2016;155:376–386.
6. Hanna E, DeMonte F, Ibrahim S, Roberts D, Levine N, Kupferman M. Endoscopic resection of sinonasal cancers with and without craniotomy: oncologic results. *Arch Otolaryngol Head Neck Surg* 2009;135:1219–1224.
7. Cracchiolo JR, Patel K, Migliacci JC, et al. Factors associated with a primary surgical approach for sinonasal squamous cell carcinoma. *J Surg Oncol* 2018;117:756–764.
8. Jafari A, Shen SA, Qualliotine JR, Orosco RK, Califano JA, DeConde AS. Impact of margin status on survival after surgery for sinonasal squamous cell carcinoma. *Int Forum Allergy Rhinol* 2019;9:1205–1211.
9. Zhang RR, Schroeder AB, Grudzinski JJ, et al. Beyond the margins: real-time detection of cancer using targeted fluorophores. *Nat Rev Clin Oncol* 2017;14:347–364.
10. Lamberts LE, Koch M, de Jong JS, et al. Tumor-specific uptake of fluorescent bevacizumab-IRDye800CW microdosing in patients with primary breast cancer: a phase I feasibility study. *Clin Cancer Res* 2017;23:2730–2741.
11. Hoogstins CES, Boogerd LSF, Sibinga Mulder BG, et al. Image-guided surgery in patients with pancreatic cancer: first results of a clinical trial using SGM-101, a novel carcinoembryonic antigen-targeting, near-infrared fluorescent agent. *Ann Surg Oncol* 2018;25:3350–3357.
12. Burggraaf J, Kamerling IMC, Gordon PB, et al. Detection of colorectal polyps in humans using an intravenously administered fluorescent peptide targeted against c-Met. *Nat Med* 2015;21:955–961.
13. van Dam GM, Themelis G, Crane LMA, et al. Intraoperative tumor-specific fluorescence imaging in ovarian cancer by folate receptor- α targeting: first in-human results. *Nat Med* 2011;17:1315–1319.
14. Gao RW, Teraphongphom N, de Boer E, et al. Safety of panitumumab-IRDye800CW and cetuximab-IRDye800CW for fluorescence-guided surgical navigation in head and neck cancers. *Theranostics* 2018;8:2488–2495.
15. Gao RW, Teraphongphom NT, van den Berg NS, et al. Determination of tumor margins with surgical specimen mapping using near-infrared fluorescence. *Cancer Res* 2018;78:5144–5154.
16. Nishio N, van den Berg NS, van Keulen S, et al. Optimal dosing strategy for fluorescence-guided surgery with panitumumab-IRDye800CW in head and neck cancer. *Mol Imaging Biol* 2019. <https://doi.org/10.1007/s11307-019-01358-x>.
17. van Keulen S, Nishio N, Birkeland A, et al. The sentinel margin: intraoperative ex vivo specimen mapping using relative fluorescence intensity. *Clin Cancer Res* 2019;25:4656–4662.
18. van Keulen S, van den Berg NS, Nishio N, et al. Rapid, non-invasive fluorescence margin assessment: optical specimen mapping in oral squamous cell carcinoma. *Oral Oncol* 2019;88:58–65.
19. van den Berg NS, Miwa M, KleinJan GH, et al. (Near-infrared) fluorescence-guided surgery under ambient light conditions: a next step to embedment of the technology in clinical routine. *Ann Surg Oncol* 2016;23:2586–2595.
20. Valentine R, Wormald P-J. A vascular catastrophe during endonasal surgery: an endoscopic sheep model. *Skull Base* 2011;21:109–114.
21. Manjunath L, Derousseau T, Batra PS. Prognostic value of surgical margins during endoscopic resection of paranasal sinus malignancy. *Int Forum Allergy Rhinol* 2015;5:454–459.
22. Chiu AG, Ma Y. Accuracy of intraoperative frozen margins for sinonasal malignancies and its implications for endoscopic resection of sinonasal melanomas. *Int Forum Allergy Rhinol* 2013;3:157–160.
23. Terasawa M, Ishizawa T, Mise Y, et al. Applications of fusion-fluorescence imaging using indocyanine green in laparoscopic hepatectomy. *Surg Endosc* 2017;31:5111–5118.
24. Krane LS, Manny TB, Hemal AK. Is near infrared fluorescence imaging using indocyanine green dye useful in robotic partial nephrectomy: a prospective comparative study of 94 patients. *Urology* 2012;80:110–116.
25. Klapdor R, Hertel H, Hillemann P, et al. Peritoneal contamination with ICG-stained cervical secretion as surrogate for potential cervical cancer tumor cell dissemination: A proof-of-principle study for laparoscopic hysterectomy. *Acta Obstet Gynecol Scand* 2019;98:1398–1403.

26. Ushimaru Y, Omori T, Fujiwara Y, et al. The feasibility and safety of preoperative fluorescence marking with indocyanine green (ICG) in laparoscopic gastrectomy for gastric cancer. *J Gastrointest Surg* 2019;23:468–476.
27. Tummers WS, Miller SE, Teraphongphom NT, et al. Intraoperative pancreatic cancer detection using tumor-specific multimodality molecular imaging. *Ann Surg Oncol* 2018;25:1880–1888.
28. Miller SE, Tummers WS, Teraphongphom N, et al. First-in-human intraoperative near-infrared fluorescence imaging of glioblastoma using cetuximab-IRDye800. *J Neurooncol*. 2018;139:135–143.
29. Nagengast WB, Hartmans E, Garcia-Allende PB, et al. Near-infrared fluorescence molecular endoscopy detects dysplastic oesophageal lesions using topical and systemic tracer of vascular endothelial growth factor A. *Gut* 2019;68:7–10.
30. Rosenthal EL, Warram JM, de Boer E, et al. Safety and tumor specificity of cetuximab-IRDye800 for surgical navigation in head and neck cancer. *Clin Cancer Res* 2015;21:3658–3666.
31. Nishio N, van den Berg NS, van Keulen S, et al. Optical molecular imaging can differentiate metastatic from benign lymph nodes in head and neck cancer. *Nat Commun* 2019;10:5044.